ELSEVIER

Journal of Alloys and Compounds 455 (2008) 87–91

Journal of ALLOYS AND COMPOUNDS

www.elsevier.com/locate/jallcom

# Magnetic properties and viscosity effect of $L1_0$ FePt film with GePt underlayer

J.L. Tsai *, C.J. Hsu

*Department of Materials Engineering, National Chung Hsing University, 250 Kuo Kuang Road, Taichung 402, Taiwan*

Received 20 December 2006; received in revised form 29 January 2007; accepted 30 January 2007
Available online 6 February 2007

**Abstract**

We explored the GePt underlayer thickness effect on the magnetic properties and microstructure of $L1_0$ FePt film. The GePt underlayer was deposited on quartz at 800 °C and the thickness changed from 10 to 120 nm. The $Ge_2Pt_3$ compound was formed and the island-like structure was able to relax the growth stress between $Ge_2Pt_3$ and quartz when the thickness is smaller than 60 nm. After FePt deposition, the bilayer was post-annealed at 400 °C. In plane coercivity ($H_c$) decreased from 14 to 2 kOe when the underlayer thickness increased from 10 to 120 nm. First, we suggested $L1_0$ FePt film is higher ordered ($S = 0.71$–$0.93$) on the island-like underlayer and the coercivity are larger than 8 kOe. It is because the island-like $Ge_2Pt_3$ induced tensile stress on FePt, which enhanced the formation of ordered FePt. The obstacles or pinning sites created by $Ge_2Pt_3$ island-like surface morphology makes FePt domain wall motion lagging and the coercivity become larger. But the inter-diffusion effect still exists for film with 10 nm $Ge_2Pt_3$ underlayer at 400 °C. Second, with underlayer thickness 120 nm, the Ge atoms diffused into the FePt film that suppressed the ordering with parameter $S = 0.49$ and the coercivity was 2 kOe.


*Keywords:* $L1_0$ FePt; Coercivity; Island-like

## 1. Introduction

The $L1_0$ FePt film has considerable as a potential candidate for ultrahigh density magnetic recording media because of its high uniaxial magnetocrystalline anisotropy energy. In $L1_0$ alloy, the FePt system presents highly coercivity, good corrosion resistance, large magnetic energy product but high temperature annealing is required to transform fcc disordered structure to $L1_0$ ordered FePt phase. For single crystalline FePt film, a very large coercivity 100 kOe was found in thin island-like grown film [1]. However, the coercivity drops to 2 kOe when the film become continuous with thickness more than 40 nm, because there are few domain wall pinning sites in single crystal film. It is easy to obtain high coercivity in continuously FePt polycrystalline films due to the twins, anti-phase boundary as domain wall pinning sites [2]. In addition, the multitwin can be introduced from the Pt/FePt interface. These results imply the underlayer plays a significant role for FePt magnetic properties. In previous reports, ordering temperature can be reduced by many ways: using a proper underlayer, for example, $Cr_{91}Ru_9$, MgO, $Cu_3Si$, etc. [3–5], addition of the third element such as Ag, Cu, Zr, etc. [6,7], alternating monatomic layer deposition, Ag top layer effect, annealing of multilayer, and ion irradiation [8–10]. The ordered AuCu and MnPt underlayer have also been used to reduce the ordering temperature of FePt films [11,8]. The mechanism of lower ordering temperature comes from the stress, defects, lattice distortion or surface roughness which promoted phase transformation.

In this study, we used $Ge_2Pt_3$ underlayer to create different surface morphology and explored the underlayer thickness effect on the magnetic properties of FePt film. Related studies report that nanocrystralline Ge, GeFe particles embedded in $SiO_2$ matrix at the evaluated temperature. We discussed the $L1_0$ FePt ordering with discontinuous or continuous GePt underlayer at fixed post-annealing temperature 400 °C. We considered the inter-diffusion effect between FePt and GePt by depth profile curves. Magnetic viscosity measurements have been proposed as a way to understand the magnetization reversal process in hard magnetic materials [12]. In previous work, we discussed the magnetic viscosity effect of FePt on island-like GePt (20 nm)

* Corresponding author. Tel.: +886 4 22875741; fax: +886 4 22857017.
*E-mail address:* tsaijl@dragon.nchu.edu.tw (J.L. Tsai).

0925-8388/$ – see front matter © 2007 Elsevier B.V. All rights reserved.
doi:10.1016/j.jallcom.2007.01.157

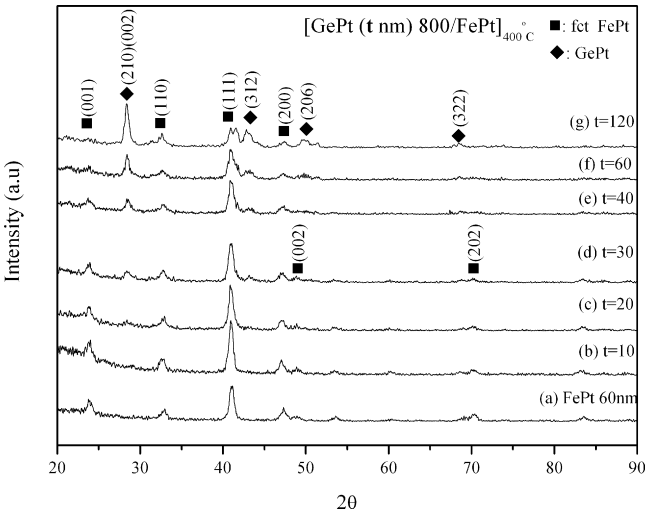


Fig. 1. XRD patterns of [FePt/GePt($t$ nm)]$_{400\,°C}$ bilayer with $t$ = 10–120 nm.

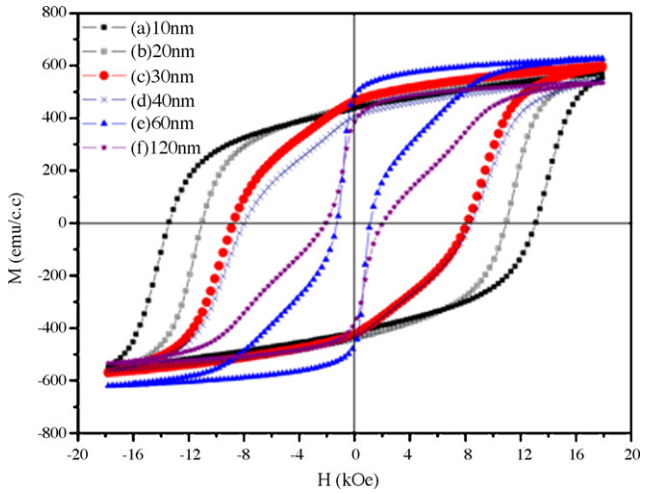


Fig. 2. Hysteresis loops of [FePt/GePt($t$ nm)]$_{400\,°C}$ bilayer with $t$ = 10–120 nm.

underlayer [13,14]. When the post-annealing temperature of (FePt/GePt) bilayer increased up to 800 °C, all islands are isolated completely. In this article, the post-annealing temperature was fixed at 400 °C and we study continuous FePt film on island-like to continuous GePt underlayer. Furthermore, we explored the thermal activation effect of FePt film on different GePt surface morphology. The experimental curves ($S_0$ versus $H$) are fitted to the simulated curves by using analytical model proposed by Chantrell et al. [15].

## 2. Experimental

The [FePt(RT)/GePt($d$ °C)]$_{p\,°C}$ ($d$: being the deposition temperature; $p$: being the post-annealing temperature) bilayer were prepared by RF magnetron sputtering. The base pressure of the chamber was about $10^{-7}$ Torr and the working pressure was 10 mTorr with high purity argon gas. The composite FePt target was fabricated by embedding Pt square foils on the circular Fe plate (2 in. in diameter). The similar method was also used in preparing GePt target. The underlayer and film chemical composition were Ge:Pt = 40.2:59.8 (at.%), Fe:Pt = 54.9:46.1 (at.%), respectively, and performed by inductively coupled plasma (ICP) spectroscopy. The underlayer $Ge_2Pt_3$ was deposited on the quartz substrate with varied thickness ($t$ = 10–120 nm) at $d$ = 800 °C and annealing for half an hour. Then FePt with fixed thickness 60 nm was grown on the underlayer that has been cooled down to the room temperature. After deposition, the bilayer FePt/GePt films were post annealing at $p$ = 400 °C for 1 h. The film crystal structure was investigated by a grazing incident X-ray diffractometry (XRD) with Cu Kα radiation (λ = 0.1541 nm) and small slits (0.10 mm for divergent slit; 4 mm for scattering slit and receiving slit). The film microstructure was observed by transmission electron microscopy (TEM). The depth-profile of the films was examined by auger electron spectroscopy (AES) with $Ar^+$ etching. Magnetic hysteresis loops were measured at room temperature by using vibration sample magnetometer (VSM) with the maximum magnetic field of 1.8 T.

## 3. Results

### 3.1. A. GePt underlayer thickness effect on $L1_0$ FePt film

Fig. 1 shows a series of grazing incident XRD patterns of films with varied GePt underlayer thickness. Fig. 1(a) shows the FePt single layer film, the superlattice peaks (0 0 1) and (1 1 0) and fundamental peaks (1 1 1), (2 0 0), (2 0 2) were indexed that belong to ordered face-centered-tetragonal (fct) $L1_0$ FePt phase. The (0 0 1), (2 0 0) and (2 0 2) peaks intensity decreased as the GePt underlayer thickness increased and broaden shown in Fig. 1(g). Also, we found the (2 1 0), (0 0 2) diffraction peaks that belong to $Ge_2Pt_3$ phase when the underlayer thickness above 30 nm. The lattice parameter $c/a$ ratio can be determined by FePt $L1_0$ phase in X-ray diffraction peaks (0 0 1), (1 1 0). The long-range order parameter ($S$) can be estimated as $S^2 = (1 - c/a)/[1 - (c/a)_{Sf}]$ and the composition deviation has also been considered. The $(c/a)_{Sf}$ is 0.965 for the fully ordered($S_f$) $Fe_{51}Pt_{49}$ films at 800 °C. The ordering parameter decreased from 0.93 to 0.49 when the GePt thickness increased from 10 to 120 nm. Fig. 2 shows the FePt/GePt bilayer room temperature magnetic hysteresis loops. We found that the coercivity of films were strongly dependent on the GePt underlayer thickness or ordering parameter. With underlayer thickness $t$ = 10 nm, the maximum coercivity 14 kOe was obtained. In comparison, the minimum coercivity 2 kOe was obtained with thicker underlayer $t$ = 120 nm.

In order to examine the diffusion at the interface, AES depth profiles of the samples with GePt underlayer thickness 10 and 120 nm were done, as illustrated in Fig. 3. For both samples, the oxygen diffused from the film surface, which may be caused by the grain boundary diffusion and $Ar^+$ bombardment effect. In Fig. 3(a), some Ge atoms diffused from the underlayer and there was a narrow intermixing region between the interface of FePt and GePt and it is a Ge-rich FePt film. As a result, the coercivity was not influenced by diffusion. However, in Fig. 3(b), the Ge atoms diffused deeply into the FePt film. It is also a main reason of lower coercivity (2 kOe) shown in Fig. 2(f). The interdiffusion effects were observed in both samples in Fig. 3 but the $H_c$ was deteriorated only for sample with GePt underlayer 120 nm. Another $Ge_3Pt_2$ underlayer surface morphology effect has been proved by atomic force microscopy (AFM) images in the previous work [16]. When post-annealing at 400 °C, the (GePt($t$ < 60 nm)/FePt) bilayer presents island-like surface morphology with each island connected closely and the magnetic domain structure looks continuous. When the GePt thickness is up to 60 nm, the bilayer exhibits continuous surface morphology and continuous stripe domains.

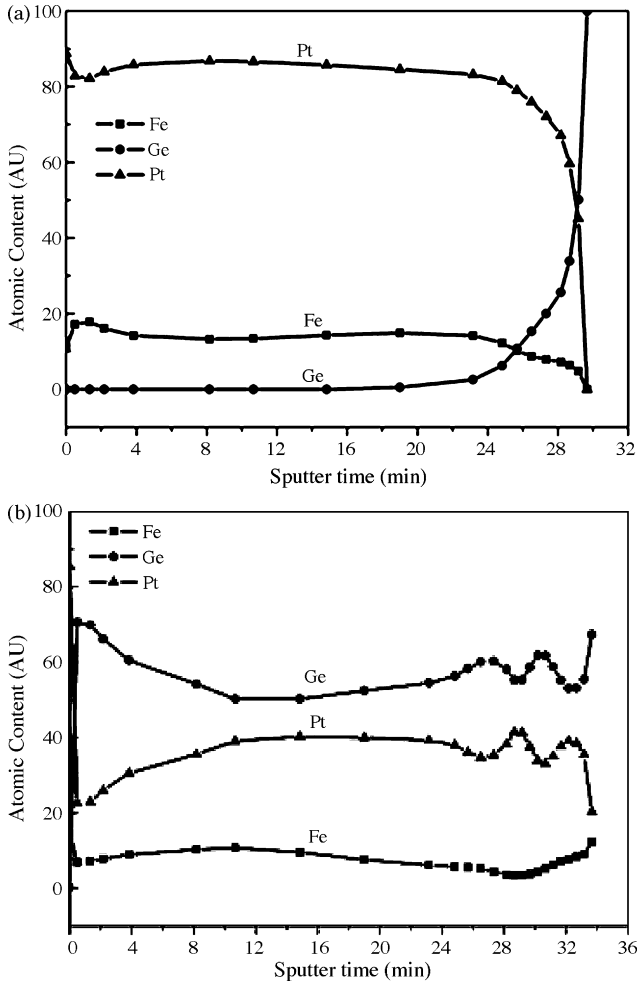


Fig. 3. AES depth profiles of the samples with GePt underlayer thickness 10 and 120 nm.

Fig. 4(a) shows the bright field image of GePt underlayer with thickness 20 nm and annealed at 800 °C. The island-like structure was observed and the average size of each island was 100 nm. When the GePt thickness increased up to 60 nm, the films become continuously. As a result, different GePt surface roughness and stress field distribution were supplied before FePt deposition. Fig. 4(b) shows the bright field image of $[FePt(RT)/GePt(800\,^{\circ}C)]_{400\,^{\circ}C}$ bilayer. The FePt film should be deposited on the $Ge_2Pt_3$ particle-like structure or the quartz matrix simultaneously. After post annealing at 400 °C for 1 h, the $Ge_2Pt_3$ grain growth and the $L1_0$ FePt ordering was finished. More interesting, the coercivity of $[FePt(RT)/GePt(800\,^{\circ}C)]_{400\,^{\circ}C}$ bilayer is much larger than the single layer FePt film under the same process. It can be explained by two areas FePt films in Fig. 4(b). For FePt in area (I), the $Ge_2Pt_3$ island structure plays as pinning sites during domain wall motion. However, in area (II), some FePt single domain particles can be formed within 100 nm and the magnetization reversal was contributed by domain wall motion or rotation at the same time. For reference, Fig. 4(c) shows the FePt single layer image under the same deposition condition [14].

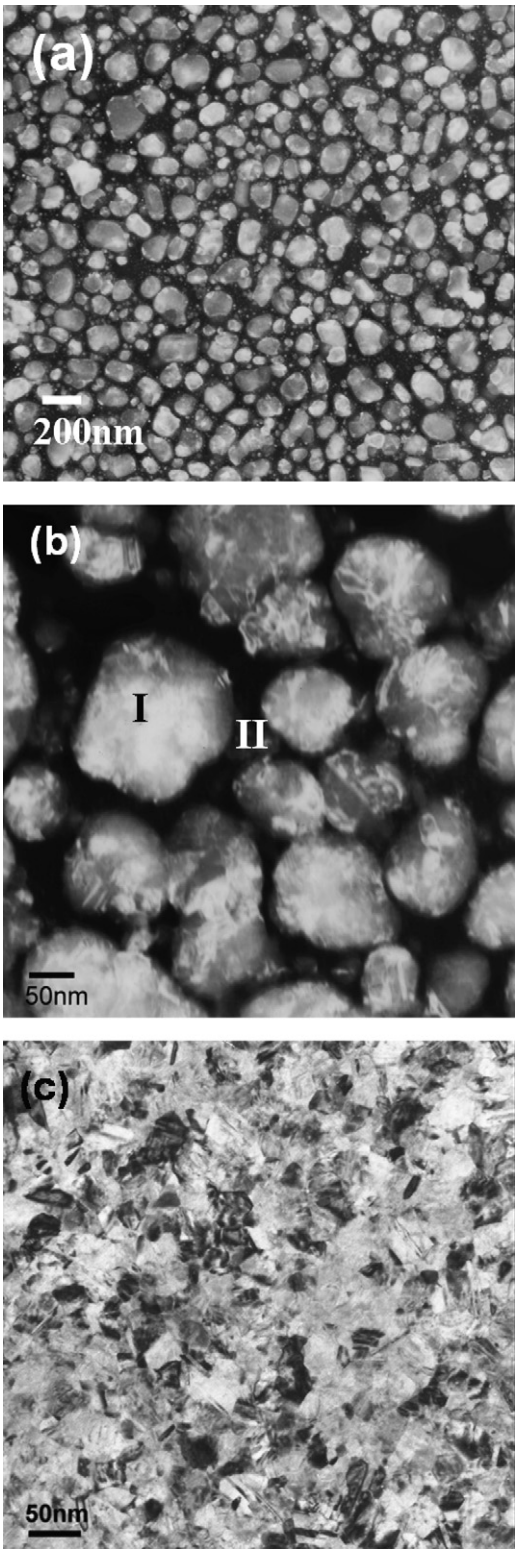


Fig. 4. TEM bright field images of (a) GePt single layer, (b) $[FePt/GePt]_{400\,^{\circ}C}$ bilayer, and (c) FePt single layer (Ref. [13]).

### 3.2. B. Magnetic viscosity measurement

From the TEM observation above, different $Ge_2Pt_3$ underlayer morphology makes different kinds of FePt microstructure. In Fig. 4(b), the FePt grains were attributed on the island-like

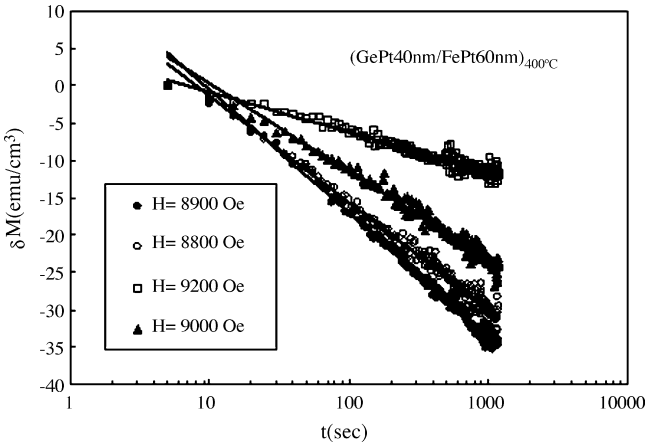


Fig. 5. Magnetization as a function of time under different reversed fields.

$Ge_2Pt_3$ or quartz substrate simultaneously and the grain sizes distribution should be wider. Furthermore, the grain size influenced the FePt film coercivity and the thermal activation of small grains becomes important. To study this effect, the magnetic viscosity measurement was performed. Fig. 5 shows the magnetization decay as a function of logarithmic time at certain reversed field near coercivity and we found the linear relationship between magnetization ($M$) and log($t$). Here the magnetic viscosity coefficient ($S_0$) was determined by the slope in Fig. 5. It was recognized by Street [17] that the exponential decay of magnetization arises from a distribution in the energy barrier. Since the dependence of energy barrier on the respective relaxation time is logarithmic. Fig. 6 shows the $S_0$ values plot as a function of applied field ($H$). The curve shows the bell shape except sample [FePt/GePt (120 nm)] and the maximum $S_0$ value was obtained at the coercivity ($H_c$) field because of the minimum energy barrier, that is, of irreversible transition from metastable to stable states, under the constant field conditions. Comparing to the previous work [13], well bell shape in $S_0$ versus $H$ curve can be obtained in high ordered FePt film with higher coercivity. One experimental curve was fitted to the simulated curve based on the analytical model proposed by Chantrell et al. [15] and the details were described in previous paper [13]. The standard

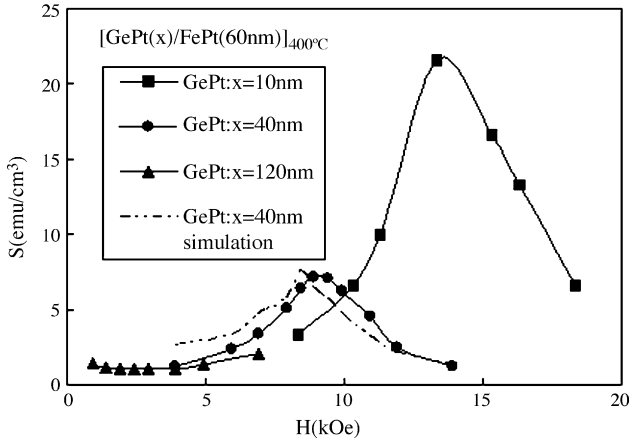


Fig. 6. Magnetic viscosity coefficient as a function of applied reversed filed for FePt/GePt bilayer with different underlayer thickness.

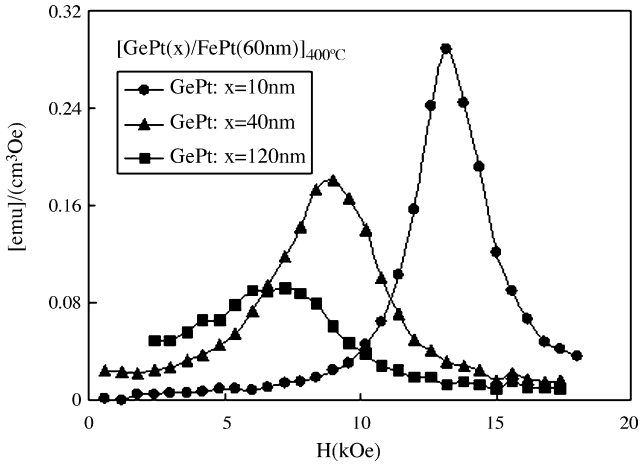


Fig. 7. Irreversible susceptibility as a function of applied filed for FePt/GePt bilayer.

deviation $\sigma = 2$ is treated as the fitting parameter. This value is a little higher than our previous work [13] $\sigma = 0.7$, because the ordering or coercivity is lower in thicker GePt underlayer (40 nm > 20 nm), and we cannot get the well bell shape in $S_0$–$H$ curve.

The irreversible change of the magnetization $dM_{irr}$ can be induced by the change in the applied field $dH$. And the irreversible susceptibility ($\chi_{irr}$) can be derived by measuring the dc demagnetization (DCD) curve (or magnetization recoil curve). The switching field distribution curve $\chi_{irr}$, which was obtained by differentiating the dc demagnetization curve. Fig. 7 shows the plot of $\chi_{irr}$ as a function of applied field. The curve shows the similar bell shape and with the maximum value at the coercivity field. The similar shape of the $S_0(H)$ and $\chi_{irr}(H)$ curves suggested that the thermal activation plays an important role in magnetization reversal process. The field dependence of the activation volumes were estimated by $V_a = (k_B T \chi_{irr})/(M_s S_0)$. Here the ratio of $S_0/\chi_{irr}$ was defined as the fluctuation field $H_f = 39.5$ Oe at $H_c$ for sample with underlayer thickness 40 nm. The activation volumes $V_a = 1.05 \times 10^{-18}$ cm$^3$ are smaller than the average physical grain size observed in TEM. This value is reasonable in between the $V_a = (0.5–1.9) \times 10^{-18}$ cm$^3$ in previous work [13].

In summary, the island-like $Ge_2Pt_3$ underlayer (with thickness <60 nm) supplied more surface roughness and strain energy for FePt ordering. Also we obtained the higher coercivity and ordering on discontinuous GePt underlayer. But the interlayer diffusion effect still exists when the GePt underlayer thickness is smaller than 60 nm. However, interlayer diffusion becomes the main reason to suppress the ordering with 120 nm $Ge_2Pt_3$ underlayer. Finally, we investigated the thermal activation behavior of films with fruitful microstructure by magnetic viscosity.

## Acknowledgement

This work was sponsored by the National Science Council of Republic of China under Grant no. NSC 95-2221-E-005-027.

## References

[1] T. Shima, K. Takanashi, Y.K. Takahashi, K. Hono, Appl. Phys. Lett. 85 (2004) 2571.
[2] Y.K. Takahashi, T.O. Seki, K. Hono, T. Shima, K. Takanashi, J. Appl. Phys. 96 (2004) 475.
[3] J.S. Chen, B.C. Lim, J.P. Wang, J. Appl. Phys. 93 (2003) 8167.
[4] C.H. Lai, C.H. Yang, C.C. Chiang, T. Balaji, T.K. Tseng, Appl. Phys. Lett. 85 (2004) 4430.
[5] J.U. Thiele, L. Folks, M.F. Toney, D.K. Weller, J. Appl. Phys. 84 (1998) 5686.
[6] R.F.C. Farrow, D. Weller, R.F. Marks, M.F. Toney, A. Cebollada, G.R. Harp, J. Appl. Phys. 79 (1996) 5967.
[7] T. Shima, K. Takanashi, Y.K. Takahashi, K. Hono, Appl. Phys. Lett. 88 (2006) 063117.
[8] T. Maeda, T. Kai, A. Kikitsu, T. Nagase, J. Akiyama, Appl. Phys. Lett. 80 (2002) 2147.
[9] D. Ravelosona, C. Chappert, V. Mathet, H. Bernas, Appl. Phys. Lett. 76 (2000) 236.
[10] I.D. Sharp, D.O. Yi, Q. Xu, C.Y. Liao, J.W. Beeman, E.E. Haller, et al., Appl. Phys. Lett. 86 (2005) 063107.
[11] K. Barmak, J. Kim, D.C. Berry, K.W. Wierman, E.B. Svedberg, J.K. Howard, J. Appl. Phys. 95 (2004) 7486.
[12] S.T. Chui, J. Magn. Magn. Mater. 217 (2000) 120.
[13] J.L. Tsai, C.J. Hsu, J. Phys. Condens. Mat. 18 (2006) 7729.
[14] C.J. Hsu, J.L. Tsai, C.W. Hsu, S.K. Chen, W.C. Chang, IEEE Trans. Magn. 18 (2006) 7729.
[15] R.W. Chantrell, A. Lyberatos, M. El-Hilo, K. O'Grady, J. Appl. Phys. 76 (1994) 6407.
[16] J.L. Tsai, C.J. Hsu, J. Alloy Compd. 426 (2006) 426–431.
[17] R. Street, S.D. Brown, J. Appl. Phys. 76 (10) (1994) 6386.